Mathematics

AIMS Mathematics, 7(11): 19822–19845.
DOI: 10.3934/math.20221086
Received: 18 May 2022
Revised: 18 August 2022
Accepted: 22 August 2022
Published: 08 September 2022

http://www.aimspress.com/journal/Math

Research article

Activation energy impact on unsteady Bio-convection nanomaterial flow over porous surface

Madeeha Tahir[1], Ayesha Naz[2], Muhammad Imran[2,*], Hasan Waqas[2], Ali Akgül[3,4,*], Hussein Shanak[5], Rabab Jarrar[5] and Jihad Asad[5]

[1] Department of Mathematics, Government College Women University, Faisalabad 38000, Pakistan
[2] Department of Mathematics, Government College University, Faisalabad 38000, Pakistan
[3] Siirt University, Art and Science Faculty, Department of Mathematics, Siirt 56100, Turkey
[4] Near East University, Mathematics Research Center, Department of Mathematics, Near East Boulevard, PC 99138, Nicosia /Mersin 10, Turkey
[5] Department of Physics, Faculty of Applied Sciences, Palestine Technical University-Kadoorie, Tulkarm P 305, Palestine

* **Correspondence:** Email: drmimranchaudhry@gcuf.edu.pk, aliakgul00727@gmail.com.

Abstract: Nanofluid is an advanced technology to enhance heat transportation. Additionally, the thermal conductivity of nanofluids is high therefore, they are more useful for heat transportation. Evaluation of entropy generation has been a helpful technique for tackling improvements in thermal features because it provides information that cannot be obtained via energy analysis. For thermodynamic irreversibilities, a good approximation is the rate of entropy generation. As a result of a reduction of entropy production, energy transport infrastructure has become more efficient. This study aims to analyse the bioconvective flow of nanofluid flow through a stretching sheet in the occurence of gyrotactic motile microorganisms. A magnetised nanomaterial model with thermophoretic and Brownian diffusion properties is analysed. The impacts of activation energy, temperature dependent and exponential base heat source are investigated in this analysis. The entropy generation of the system is also observed for nanofluid flow. The mathematical model is developed as partial differential equations. The governing equations are reduced to a dimensionless system of ordinary differential equations by applying similarity transformations. The ODEs are tacked numerically with the aid of shooting scheme in commercial software MATLAB. For graphical and numerical results of flow controlling parameters versus subjective fields, the commercial software MATLAB tool bvp4 is used with the shooting scheme. The novelty of this analysis computes numerical computation of bioconvective nanofluid flow with temperature-dependent and exponential base heat source investigated. Furthermore, the consequence of thermal radiation and entropy of the system is considered. The porous medium with activation energy is also taken into consideration. The results show that the velocity field is reduced with increased bioconvection Rayleigh number. The thermal field is increased via an exponential space-based heat source. The concentration is reduced via Lewis number. the microorganisms profile declines for larger bioconvection Lewis number. The Brinkman number Br, magnetic and permeability characteristics all showed a rising trend when plotted against the entropy production rate.

Keywords: bioconvection; thermal conductivity; mixed convection; entropy generation; nonlinear Radiation
Mathematics Subject Classification: 74F05, 76S05

1. Introduction

Nanofluid is a revolutionary heat transfer medium that consists of nanoscale particles distributed in base liquids in a homogenous and stable manner. Nanofluid is the diluted expansion of nanoparticles in liquid. The thermal (conductivity, performance) of conventional materials is greatly improved by these distributed nanoscale particles composed of metal oxide or metal. Recent developments in nanofluid theory demonstrate unequivocally that nanoscale liquids efficiently improve the thermal properties of traditional heat carrier materials. Nanofluids are utilised for liquid cooling computer processors' excellent thermal conductivity. The stability and dispersion of nanoparticles in the system determine the efficiency of nanofluid. The thermophysical characteristics that predict heat transfer behaviour are critical for energy-saving and industrial applications. Nanofluid is also used to clean up pollutants for medicinal purposes, cooling vehicle engines, and cooling effective heat equipment. Medical engineering uses of nanofluids are getting a lot of interest. Some research topics include pharmacodynamics [1] and biofuel cells with plant inspiration [2]. In particular, applications for bio-inspired proton exchange membrane (PEM) fuel cells are growing [3]. Various studies have been conducted on nanofluids from different perspectives. In 1995, Choi and Eastman [4] gave the concept of nanofluids. Low thermal conductivity is a stumbling block in the progression of energy-efficient heat transport fluids that are needed in many industrial applications. Choi used nanofluid to improve material thermal conductivity. Wen and Ding [5] formulated the nanofluid by soaking titanium dioxide nanoparticles in filtered water, which is highly stable, and investigating their heat transfer actions under natural convection conditions. Buongiorno [6] proposed two essential features to increase heat transfer in nanomaterials: Brownian motion and thermophoretic diffusion. Murshed et al. [7] made a composite experimental and theoretical analysis of nanofluid's sensitive thermal conductivity and viscosity. They observed that nanofluid's thickness and thermal conductivity increase the thickness of the nanoparticle volume fraction. Ganguly et al. [8] used aluminium oxide nanoparticles in their research and found that electrical conductivity enhanced with increased volume fraction and temperature. Kuznetsov and Nield [9] utilised the Buongiorno model to investigate the convective flow along a vertical plate. Mustafa et al. [10] discussed the nanofluid's flow approaching a stagnation point towards a surface that has been stretched. Natural convective heat transfer of Ethylene Glycol nanofluids across a thin platinum wire was scrutinized by Asadzadeh et al. [11]. They discovered that the nanomaterials added to ethylene glycol boosted heat transmission up to 0.02 percent volume fraction. Hayat et al. [12] analysed thixotropic nanofluid in the direction of an inflexible stretching surface. Farooq et al. [13] intrigued viscoelastic nanofluid's over a stretched surface having non-linear radiative impacts. Bhatti et al. [14] worked on Jeffrey nanofluid. They explored the effect of clotting and a changing magnetic field on non-Newtonian fluid peristaltically generated motion, considering gyrotactic microbes across an annulus. Khan et al. [15] discussed the consequence of non-linear radiative MH flow of a Cross nanofluid in the flow towards a stretched surface. Nadeem et al. [16] investigated the Hybrid nanofluid's via a circular cylinder while taking thermal slip into account. Bhatti et al. [17] introduced the hybrid nanofluid flow. Bhatti et al. [18] disclosed the stagnation point nanofluid flow and magnetohydrodynamic effect over the stretchable sheeet. Rashidi et al. [19] analysed the statistical analysis of thermal conductivity nanofluid flow. Many researchers are intrested in the investigation about MHD nanofluid flow with heat tranfar and viscous desipation effect [20–24] against stretchable surface. Upreti et al. [25] explored the Sisko nanofluid flow with viscous dissipation behavior on stretchable surfaces. Joshi et al. [26] deliberated the impact of thermal radiative MHD flow and suction/blowing velocity on the hybrid-based nanofluid on a stretching sheet. Upreti et al. [27] scrutinized 2-dimensional nanofluid flow with single walled and multi walled carbon nanotubes versus a horizontal porous plate. Joshi et al. [28] examined the magnetically hybrid-based 3D nanofluid flow under the mixed convection phenomena against a porous bidirectional stretching sheet due to the physical properties of a higher - order binary chemical reaction, interior heat generation. Rawat et al. [29] observed the heated stratified Cattaneo-Christov heat flux nanofluidic flow through cone. Rawat et al. [30] explored a hybrid-type MHD nanofluid with boundary layer flow versus a horizontal vertically plate has been established.

The 2nd rule of thermodynamics is often utilized to measure irreversibility (entropy generation). Entropy generation identifies the extent of irreversibility that occurs during any heating process. In a thermodynamic system, the quantity of entropy produced during irreversible processes is referred to as entropy generation. The amount of appropriate work destroyed during the process is directly proportional to the irreversibility of the process. The entropy generation connects fluid mechanics, the fundamental thermodynamic concepts, and heat transfer. These entropy-generating sources are applied to the enhancement and design of actual structures and methods constrained by (finite, temporal) limitations, heat/mass transfer, and irreversibilities in fluid flow. The primary aim of researchers in most engineering and industrial implimentations is to decline entropy formation to improve efficiency and effectiveness. Firstly, Bejan [31] explored entropy generation in a convective heat transport mechanism. Bejan [32] demonstrates that the flow geometry factors directly correlate with the degree of irreversibility of a convective heat transfer mechanism. Bejan discovered that two distinct characteristics, namely liquid friction and heat transfer owing to a temperature gradient, are responsible for entropy generation in the process of fluid flow. Also, the uses of a number that minimises irreversibility on a multidimensional level are outlined. However, the entropy creation rate must be reduced for thermodynamic functioning to be feasible. Bejan [33] also discussed the minimisation of entropy generation for modelling and optimising real-world systems utilising integrated heat transport and thermodynamics. Tasnim et al. [34] investigated entropy production inside the vertical slit formed by two parallel plates immersed in a porous material and subjected to the hydromagnetic effect. Mahmud and Fraser [35] worked on convective heat transfer problems. Ellahi et al. [36] explored various convection boundary layer flow across an inverted cone by evaluating entropy generation and nanofluid's shape impacts nanosize particles. The effect of heat radiation on entropy production in two-dimensional unsteady MHD nanofluid flow through a porous material was investigated by Shit et al. [37]. Sheikholeslami et al. [38] examined turbulent heat transfer of homogenous nanofluid considering entropy generation by inserting double twisted tapes and utilising nanomaterial. Specific recent research on the influence of entropy production is described in the references [39–49] and some studies within.

Bioconvection is the process utilised to explain the hazy pattern of uncertainty generated by low-density microorganisms swimming in the upper section of the fluid. By incorporating microorganisms into nanofluid, the suspension's stability increases. Bioconvection is a natural phenomenon due to the random movement of microorganisms in a single-celled or cell-form colony. Upswimming microorganisms are of two categories that are ordinarily employed in bioconvection experiments-heavy alga and certain oxytactic bacteria. These bacteria are known as gyrotactic microorganisms because they have a higher density than water and seem to cluster on the top section of the fluid. In 1996, by suspending microscopic swimming microbes, Vincent and Hill [50] investigated the mechanism of bioconvection. Kuznetsov [51] suggested the evolution of micro-organisms in micro-microsystems with a significant role in mass transfer production and stockpiling. Alqarni et al. [52] analyzed the impact of bioconvection nanofluid on magnetized two dimensional flows via lubricated surface with the presence of melting phenomenon and gyrotactic motile micro-organisms. Alluguvelli et al. [53] discussed the bioconvective nanofluid through the enclosure with the effect of viscous dissipation. Researchers [54–57] are giving much attention to nanoparticle bioconversion phenomenons.

The latest investigation adds to the work of Khan et al. [58], who scrutinized entropy generation in mixed convection nanomaterial flow. We added bioconvection and activation energy into the nanomaterial. We then used a simple and efficient computational method shooting technique in MATLAB software to solve the modelled nonlinear ordinary differential equations. The computed results for the physical quantities of interest are presented in graphical and tabular formats.

2. Formulation of mathematical model and flow analysis

Assume the effect of entropy generation on bioconvective nanofluid flow across a stretching porous surface in the presence of motile microorganisms. The nonlinear thermal radiation, temperature base heat sink and exponential space-based heat source are considered. The velocity slip is also taken into account. A Buongiorno model for nanofluid, which tackles Brownian and thermophoretic diffusions effect, is taken into account. The famous Darcy relation for developing porous media properties is used. The mathematical model's flow pattern is detailed in Figure 1.

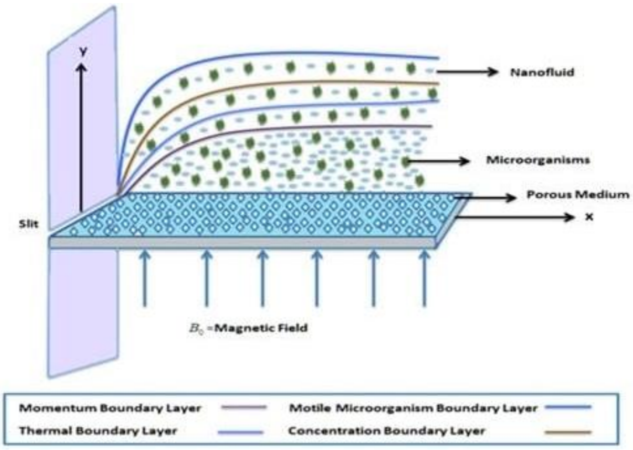

Figure 1. Geometry of flow.

The governing equations for the flow mentioned above problem are [58]

$$\frac{\partial \bar{u}}{\partial x}+\frac{\partial \bar{v}}{\partial y}=0, \tag{1}$$

$$\begin{aligned}\frac{\partial \bar{u}}{\partial t}+\bar{u}\frac{\partial \bar{u}}{\partial x}+\bar{v}\frac{\partial \bar{u}}{\partial y}&=-\frac{1}{\rho}\frac{\partial p}{\partial x}+\nu\frac{\partial^2 \bar{u}}{\partial y^2}-\frac{\sigma}{\rho}B_0^2\bar{u}-\nu\frac{\bar{u}}{\kappa_p}\\&+\frac{1}{\rho_f}g^*\begin{bmatrix}\left(1-C_f\right)\rho_f\beta^{**}\left(\bar{T}-\bar{T}_\infty\right)-\left(\rho_p-\rho_f\right)\left(\bar{C}-\bar{C}_\infty\right)\\-\left(\bar{N}-\bar{N}_\infty\right)\gamma^*\left(\rho_m-\rho_f\right)\end{bmatrix},\end{aligned} \tag{2}$$

$$\frac{\partial p}{\partial y}=0, \tag{3}$$

$$\begin{aligned}\frac{\partial \bar{T}}{\partial t}+\bar{u}\frac{\partial \bar{T}}{\partial x}+\bar{v}\frac{\partial \bar{T}}{\partial y}&=\frac{\alpha_m}{(\rho c)_f}\frac{\partial^2 \bar{T}}{\partial y^2}+\frac{\sigma B_0^2}{(\rho c)_f}\bar{u}^2+\frac{\nu}{c_p}\left(\frac{\partial \bar{u}}{\partial y}\right)^2+\frac{Q_t}{(\rho c)_f}(\bar{T}-\bar{T}_\infty)\\&+\frac{Q_e}{(\rho c)_f}(\bar{T}_w-\bar{T}_\infty)exp\left(-\sqrt{\left(\frac{\bar{u}_0}{2\nu L(1-\lambda t)}\right)}e^{\frac{x}{2L}}ny\right)+\bar{\tau}\left[\bar{D}_B\frac{\partial \bar{T}}{\partial y}\frac{\partial \bar{C}}{\partial y}+\frac{\bar{D}_T}{\bar{T}_\infty}\left(\frac{\partial \bar{T}}{\partial y}\right)^2\right]-\frac{1}{(\rho c)_f}\frac{\partial q_r}{\partial y},\end{aligned} \tag{4}$$

$$\frac{\partial \bar{C}}{\partial t}+\bar{u}\frac{\partial \bar{C}}{\partial x}+\bar{v}\frac{\partial \bar{C}}{\partial y}=\bar{D}_B\frac{\partial^2 \bar{C}}{\partial y^2}+\frac{\bar{D}_T}{\bar{T}_\infty}\frac{\partial^2 \bar{T}}{\partial y^2}-k_r^2(\bar{C}-\bar{C}_\infty)\left(\frac{\bar{T}}{\bar{T}_\infty}\right)^n e^{-\frac{E_a}{k\bar{T}}}, \tag{5}$$

$$\frac{\partial \bar{N}}{\partial t}+\bar{u}\frac{\partial \bar{N}}{\partial x}+\bar{v}\frac{\partial \bar{N}}{\partial y}+\frac{b_m W_c}{(\bar{C}_w-\bar{C}_\infty)}\left[\frac{\partial}{\partial y}\left(\bar{N}\frac{\partial \bar{C}}{\partial y}\right)\right]=\bar{D}_m\left(\frac{\partial^2 \bar{N}}{\partial y^2}\right). \tag{6}$$

Here, velocity components in (x,y) direction are symbolized by $(\bar{u},\bar{v})$. ρ and p denote density and pressure of the fluid. (μ,ν) denote (absolute,kinematic) viscosity. σ denote the respectively. B_0 is the magnetic field's strength, L denotes reference length and λ is degree of unsteadiness. c_p dessignates the specific heat, $\bar{\tau}=\frac{(\rho c)_p}{(\rho c)_f}$ characterizes the ratio of the nanoparticle's heat capacity to the base fluid's heat capacity. Q_0 denotes the coefficient of heat source/sink, α_m is thermal diffusivity, k_r^2 be a chemical reaction rate, E_a denotes the activation energy, W_c is the cell swimming speed. $(\bar{T},\bar{C},\bar{N})$ denote the temperature, concentration, and microorganisms concentration respectively. $(\bar{T}_\infty,\bar{C}_\infty,\bar{N}_\infty)$ denote the ambient (temperature, concentration, microorganisms concentration). $\bar{C}_w$ is the concentration of the surface. The coefficient of Brownian diffusion, thermophoresis, and molecular diffusion are symbolized by $(\bar{D}_B,\bar{D}_T,\bar{D}_m)$ respectively.

According to the approximation of Rosseland, the radiative heat flux is:

$$q_r = -\frac{4\sigma^*}{3k^*}\frac{\partial \bar{T}^4}{\partial z} = -\frac{16\sigma^*}{3k^*}\bar{T}^3\frac{\partial \bar{T}}{\partial y}, \tag{7}$$

in which σ^* symbolises Stefan-Boltzman constant and k^* mean absorption coefficient.

The current flow problem's boundary conditions are:

$$\begin{aligned} &\bar{u} = \bar{u}_w = (\frac{\bar{u}_0}{1-\lambda t})e^{\frac{x}{L}} + N_1\nu\left(\frac{\partial \bar{u}}{\partial y}\right),\ \bar{v} = -\bar{V}(x,t),\ -k\frac{\partial \bar{T}}{\partial y} = h_f(x,t)(\bar{T}_f - \bar{T}), \\ &D_B\frac{\partial \bar{C}}{\partial y} + \frac{D_T}{T_\infty}\frac{\partial \bar{T}}{\partial y} = 0,\ \bar{N} = \bar{N}_\infty,\ at\ y = 0, \end{aligned} \tag{8}$$

$$\bar{u} \to 0,\ \ \bar{T} \to \bar{T}_\infty,\ \ \bar{C} \to \bar{C}_\infty,\ \ \bar{N} \to \bar{N}_\infty,\ \ at\ \ y \to \infty, \tag{9}$$

where $(\bar{u}_w,\bar{u}_0)$ are the velocities of (surface, reference) and h_f be a heat transfer coefficient. $\bar{V}(x,t) > 0$ indicate suction velocity and $\bar{V}(x,t) < 0$ designate the injection velocity. Because pressure is constant along y-axis Eq (3), so there is no viscous consequence at the outer layer of the boundary. Euler's form of momentum equation can be used to calculate the pressure distribution as follows:

$$\frac{\partial \bar{u}_\infty}{\partial t} + \bar{u}_\infty\frac{\partial \bar{u}_\infty}{\partial x} = -\frac{1}{\rho}\frac{\partial p}{\partial x},$$

Where ambient velocity along the x-axis is denoted by $\bar{u}_\infty$. By using Eq (9) the ambient velocity has the following structure: $\bar{u} = \bar{u}_\infty \to 0$, and so Eq (2) becomes

$$\begin{aligned} &\frac{\partial \bar{u}}{\partial t} + \bar{u}\frac{\partial \bar{u}}{\partial x} + \bar{v}\frac{\partial \bar{u}}{\partial y} = \nu\frac{\partial^2 \bar{u}}{\partial y^2} - \frac{\sigma}{\rho}B_0^2\bar{u} - \nu\frac{\bar{u}}{\kappa_p} \\ &+\frac{1}{\rho_f}g^*\begin{bmatrix} \left(1-\bar{C}_f\right)\rho_f\beta^{**}\left(\bar{T}-\bar{T}_\infty\right) - \left(\rho_p-\rho_f\right)\left(\bar{C}-\bar{C}_\infty\right) \\ -\left(\bar{N}-\bar{N}_\infty\right)\gamma\left(\rho_m-\rho_f\right) \end{bmatrix}, \end{aligned} \tag{10}$$

To obtain the dimensionless flow pattern, the following similarity conversions are used:

$$\bar{u} = \left(\frac{\bar{u}_0}{1-\lambda t}\right)e^{\frac{x}{L}} f^{'}(\xi), \quad \bar{v} = -\sqrt{\left(\frac{\nu \bar{u}_0}{2L(1-\lambda t)}\right)}\left[f(\xi) + \xi f^{'}(\xi)\right]e^{\frac{x}{2L}},$$
$$\xi = y\sqrt{\left(\frac{\bar{u}_0}{2\nu L(1-\lambda t)}\right)}e^{\frac{x}{2L}}, \quad \psi = \sqrt{\left(\frac{2L\nu \bar{u}_0}{(1-\lambda t)}\right)}e^{\frac{x}{2L}} f\left(\xi\right), \theta = \frac{\bar{T} - \bar{T}_\infty}{\bar{T}_w - \bar{T}_\infty}, \quad \phi = \frac{\bar{C} - \bar{C}_\infty}{\bar{C}_w - \bar{C}_\infty}, \tag{11}$$
$$\chi = \frac{\bar{N} - \bar{N}_\infty}{\bar{N}_w - \bar{N}_\infty}.$$

Here stream function ψ is $\bar{u} = \frac{\partial \psi}{\partial y}$ and $\bar{v} = \frac{\partial \psi}{\partial x}$. It upholds the continuity equation Eq (1). Further Eqs (4)–(6) and Eqs (8)–(11) takes the forms:

$$f^{'''}(\xi) + f^{''}(\xi)(f(\xi) - \alpha\xi) - 2f^{'2}(\xi) - 2(K + M + \alpha) f^{'}(\xi) + 2\lambda\left(\theta - Nr\phi - Nc\chi\right), \tag{12}$$

$$\begin{aligned} &\theta^{''}(\xi) + Pr(f(\xi) - \alpha\xi + Nb\theta^{'}(\xi)\phi^{'}(\xi) + Nt\theta^{'2}(\xi)) \\ &+Rd(\theta(\xi)(\theta_w - 1) + 1)^2\{3\theta^{'2}(\xi)(\theta_w - 1) + \theta^{''}(\xi)(\theta(\xi)(\theta_w - 1) + 1))\} \\ &+Br(f^{''2}(\xi) + 2[(M + K) f^{'2}(\xi) + Q_T Pr\theta(\xi) + \Pr Q_E exp\left(-n\xi\right)]) = 0, \end{aligned} \tag{13}$$

$$\phi^{''}(\xi) + PrLe\phi^{'}[f(\xi) - \alpha\xi] + (\frac{Nt}{Nb})\theta^{''}(\xi) - PrLe\sigma(1 + \epsilon\theta)^n \phi e^{-\frac{E}{(1+\epsilon\theta)}} = 0, \tag{14}$$

$$\chi^{''}\left(\xi\right) + Lb(f\left(\xi\right) - \alpha\xi)\chi^{'}\left(\xi\right) - Pe[\phi^{''}\left(\xi\right)\left(\chi\left(\xi\right) + \Omega\right) + \phi^{'}\left(\xi\right)\chi^{'}\left(\xi\right)] = 0, \tag{15}$$

with

$$\begin{aligned} &f(0) = S,\ f^{'}(0) = 1 + \gamma f''\left(0\right), \theta^{'}(0) = -Bi(1 - \theta(0)), Nb\theta'\left(0\right) + Nt\phi'\left(0\right) = 0, \chi(0) = 1, \\ &f(\infty) = 0, \theta(\infty) = 0, \phi(\infty) = 0, \chi(\infty) = 0. \end{aligned} \tag{16}$$

In the equations above, the dimensionless variables are described as permeability parameter $K = \frac{L\nu}{\bar{u}_w \kappa_p}$, magnetic parameter $M = \frac{\sigma L B_0^2}{\rho \bar{u}_0}$, unsteadiness parameter $\alpha = \frac{L\lambda e^{-\frac{x}{L}}}{\bar{u}_0}$, mixed convection parameter $\lambda = \frac{\beta^{**} g * \mathrm{L}\left(1 - \bar{C}_\infty\right)\left(\bar{T}_w - \bar{T}_\infty\right)}{\bar{u}_w^2}$, $Nt = \frac{\tau \bar{D}_T}{\nu \bar{T}_\infty}(\bar{T}_w - \bar{T}_\infty)$ thermophoresis parameter, the bouncy ratio parameter explain with $Nr = \frac{\left(\rho_p - \rho_f\right)\left(\bar{C}_w - \bar{C}_\infty\right)}{\rho_f\left(1 - \bar{C}_\infty\right)\left(\bar{T}_w - \bar{T}_\infty\right)\beta^{**}}$, the bio convection Rayleigh number for $Nc = \frac{\gamma*\left(\rho_m - \rho_f\right)\left(\bar{N}_w - \bar{N}_\infty\right)}{\rho_f\left(1 - \bar{C}_\infty\right)\left(\bar{T}_w - \bar{T}_\infty\right)\beta^{**}}$, $Pr = \frac{(\rho c)_p \nu}{\alpha_m}$ Prandtl number, $Nb = \frac{\tau \bar{D}_B}{\nu}(\bar{C}_w - \bar{C}_\infty)$ Brownian motion variable, $Rd = \frac{16\sigma^* \bar{T}_\infty^3}{3kk^*}$ radiation variable, Brinkman number $Br = \frac{\mu c_p}{k}\frac{\bar{u}_w^2}{c_p(\bar{T}_w - \bar{T}_\infty)} = Pr.Ec$, Eckert number is $Ec=\dfrac{\bar{u}_w^2}{c_p(\bar{T}_w-\bar{T}_\infty)}$, $\theta_w=\dfrac{\bar{T}_w}{\bar{T}_\infty}$ is dimensionless temperature ratio parameter, $\delta=\dfrac{LQ_0}{\bar{u}_w\rho c_p}$ heat source/sink parameter, $Le=\dfrac{\alpha_m}{\bar{D}_B}$ Lewis number, $Lb=\dfrac{\nu}{\bar{D}_m}$ indicates bioconvection Schmidt number, $\epsilon=\dfrac{(\bar{T}_w-\bar{T}_\infty)}{\bar{T}_\infty}$ is temperature ratio variable, $E=\dfrac{E_a}{\kappa_p\bar{T}_\infty}$ is the dimensionless activation energy, $Pe=\dfrac{b_mW_c}{\bar{D}_m}$ is Peclet number, $\Omega=\dfrac{\bar{N}_\infty}{\bar{N}_w-\bar{N}_\infty}$ be the microorganisms difference parameter, $\gamma=N_1\nu\sqrt{\dfrac{\bar{u}_0}{2\nu L(1-\lambda t)}}$ and $Bi=\dfrac{h}{k}L$ is Biot number.

The drag surface force (C_f), heat transport rate Nu_x, mass transport rate Sh_x, and local density number of microorganisms Sn_x are given as:

$$C_f=\frac{\bar{\tau}_w}{\rho_f\bar{u}_w^2},\ Nu_x=\frac{Lq_w}{k(\bar{T}_w-\bar{T}_\infty)},\ Sh_x=\frac{Lj_m}{\bar{D}_B(\bar{T}_w-\bar{T}_\infty)},\ Sn_x=\frac{xj_n}{\bar{D}_m(\bar{N}_w-\bar{N}_\infty)}, \tag{17}$$

here τ_w is wall shear stress, q_w examine a heat flux, j_m denotes mass flux rate, and j_n be a motile transportation flux and are given as:

$$\bar{\tau}_w=\bar{\tau}_{xy}=\mu\left(\frac{\partial\bar{u}}{\partial y}\right)\Bigg|_{y=0},\ q_w=-k\left(\frac{\partial\bar{T}}{\partial y}\right)\Bigg|_{y=0}+(q_r)_w,\ j_m=-\bar{D}_B\left(\frac{\partial\bar{C}}{\partial y}\right)\Bigg|_{y=0},\ j_n=-\bar{D}_m\left(\frac{\partial\bar{N}}{\partial y}\right)\Bigg|_{y=0}, \tag{18}$$

using Eq (21) in Eq (17) we have

$$\begin{aligned}&Re_x^{0.5}C_f=\frac{1}{\sqrt{2}}f''(0),\ Nu_xRe_x^{0.5}=-\frac{1}{\sqrt{2}}(1+Rd(\theta(0)(\theta_w-1)+1)^3)\theta'(0),\\&Sh_xRe_x^{0.5}=-\frac{1}{\sqrt{2}}\phi'(0),\ Sn_xRe_x^{0.5}=-\frac{1}{\sqrt{2}}\chi'(0),\end{aligned} \tag{19}$$

where $Re_x=(\dfrac{L\bar{u}_w}{\nu})$ is the local Reynolds number.

3. Entropy generation

Mathematically the generation of entropy is expressed as:

$$\begin{aligned}E_g=&\frac{k}{\bar{T}_\infty^2}\left(\frac{\partial\bar{T}}{\partial y}\right)\left(1+\frac{16\sigma^*}{3k^*k}\bar{T}^3\right)^2+\frac{\mu}{\bar{T}_\infty}\left(\frac{\partial\bar{u}}{\partial y}\right)^2+\frac{\sigma B^2}{\bar{T}_\infty}\bar{u}^2+\frac{\mu}{\kappa_p\bar{T}_\infty}\bar{u}^2\\&+\frac{R\bar{D}_B}{\bar{T}_\infty}\left(\frac{\partial\bar{T}}{\partial y}\frac{\partial\bar{C}}{\partial y}\right)+\frac{RD_B}{C_\infty}\left(\frac{\partial C}{\partial y}\right)^2+\frac{R\bar{D}_B}{N_\infty}\left(\frac{\partial\bar{N}}{\partial y}\right)^2+\frac{R\bar{D}_B}{N_\infty}\left(\frac{\partial\bar{T}}{\partial y}\frac{\partial\bar{N}}{\partial y}\right).\end{aligned} \tag{20}$$

In this case, the first term on the right side of Eq (20) relates to the generation of entropy (irreversibility) via heat transfer. The second term evaluates the generation of entropy (irreversibility) due to energy dissipation in fluid friction. The third term corresponds to the entropy generation via a magnetic field and the 4th term represents entropy generation through a porous medium. The 5th and 6th terms of Eq (20) depict entropy generation (irreversibility) via mass diffusion. The final term of Eq (20) displays the generation of entropy (irreversibility) via the microorganism's concentration. The dimensionless total entropy generation rate is denoted by N_g and is given as:

$$\begin{aligned} N_g &= \theta'^2(\xi)\left(1+Rd\left(\theta(\xi)+1\right)^3\right)+\frac{Br}{\varepsilon}\left(f''^2(\xi)+2f'^2(\xi)\left(K+M\right)\right) \\ &+\frac{\Upsilon\Omega_0}{\xi}\phi'(\xi)\left(\frac{1}{\xi}\phi'(\xi)+\theta'(\xi)\right)+\left(\frac{\Gamma}{\xi}\right)^2\chi'(\xi)^2+\frac{\Upsilon_1\Omega_0}{\xi}\left(\theta'(\xi)\chi'(\xi)\right), \end{aligned} \tag{21}$$

The entropy generation due to heat transfer is

$$N_h = \theta'^2(\xi)\left(1+Rd\left(\theta(\xi)+1\right)^3\right) \tag{22}$$

The entropy generation number is represented by $N_{vjp}=\frac{Br}{\varepsilon}\left(f''^2(\xi)+2f'^2(\xi)\left(K+M\right)\right)$, the dimensionless entropy generation number for mass diffusion is represented by $N_{md}=\frac{\Upsilon\Omega_0}{\varepsilon}\phi'(\xi)\left(\frac{1}{\varepsilon}\phi'(\xi)+\theta'(\xi)\right)$, and the entropy generation number for microorganisms concentration is represented by $N_{moc}=\left(\frac{\Gamma}{\xi}\right)^2\chi'(\xi)^2+\frac{\Upsilon_1\Omega_0}{\xi}\left(\theta'(\xi)\chi'(\xi)\right)$, $Br=\frac{\bar{u}_w^2\mu}{k\left(\bar{T}_w-\bar{T}_\infty\right)}$ is Brinkman number, $\Omega=\frac{\bar{C}_w-\bar{C}_\infty}{\bar{C}_\infty}$ is dimensionless concentration ratio variable, $\varepsilon=\frac{\bar{T}_w-\bar{T}_\infty}{\bar{T}_\infty}$ is temperature ratio variable, and $\Upsilon=\frac{R\bar{D}_B\left(\bar{C}_\infty\right)}{\alpha_m}$, $\Upsilon_1=\frac{R\bar{D}_B\left(\bar{N}_\infty\right)}{\alpha_m}$ and $\Gamma=\frac{\bar{N}_w-\bar{N}_\infty}{\bar{N}_\infty}$ are dimensionless diffusion number through nanoparticles concentration. The typical rate of entropy generation is characterized by E_{g_0} and is defined as $E_{g_0}=\frac{k\left(\bar{T}_w-\bar{T}_\infty\right)^2}{\left(\frac{y}{\xi}\right)^2\bar{T}_\infty^2}$.

Bejan number Be ranges from 0 to 1. When Be fluctuates between 0 and 0.5, fluid friction irreversibility dominates. $Be=0.5$ indicates that heat transport and liquid friction produce entropy generation rates at the same rate. Be Fluctuating between 0.5 and 1 designates that heat transport irreversibility dominates. The dimensionless Bejan number is defined as:

$$Be=\frac{Entropy\,generation\,due\,to\,heat\,transfer+diffusion}{Total\,entropy\,generation}=\frac{N_h+N_{md}+N_{moc}}{N_g}. \tag{23}$$

3.1. Computational procedure

The higher order nonlinear equations with boundary are tackled numerically by implemating the bvp4c solver in MATLAB with a shooting algorithem. For this, firstly the larger higher order equations are altered to the first order problem by applying some new variables. The convergence is rate is therefore this scheme is more powerful as comppare to other numerical schemes. This technique is more efficient compare to other numerical methods. The shooting technique is utilized to convert higher order boundary value problems (BVPs) into 1st order initial value problems (IVPs).

Consider,

$$f = g_1,\ f' = g_2,\ f'' = g_3,\ f''' = g_3',\ \theta = g_4, \theta' = g_5, \theta'' = g_5',$$

$$\phi = g_6, \phi' = g_7, \phi'' = g_7', \chi = g_8, \chi' = g_9, \chi'' = g_9',$$

$$g_3' = 2g_2^2 + 2(K + M + \alpha)g_2 - g_3(g_1 - \alpha\xi) - 2\lambda\left(g_4 - Nrg_6 - Ncg_8\right) \tag{24}$$

$$\begin{aligned} g_5' = &-Pr(g_1 - \alpha\xi + Nbg_5g_7 + Ntg_5^2) - Rd(g_4(\theta_w - 1) + 1)^2\{3g_5^2(\theta_w - 1) \\ &+ g_5'(g_4(\theta_w - 1) + 1)\} - Br(g_3^2 + 2[(M + K)g_2^2])Q_T Prg_4 - \Pr Q_E exp\left(-n\xi\right), \end{aligned} \tag{25}$$

$$g_7' = -Leg_7[g_1 - \alpha\xi] - (\frac{Nt}{Nb})g_5' + PrLe\delta(1 + \epsilon g_4)^n g_6 e^{-\frac{E}{(1+\epsilon g_4)}}, \tag{26}$$

$$g_9' = Pe[g_7'\left(g_8 + \Omega\right) + g_7 g_9] - Lb[g_1 - \alpha\xi]g_9 \tag{27}$$

and the corresponding boundary constraints are:

$$\begin{aligned} &g_1(0) = S,\ g_2(0) = 1 + \gamma g_3\left(0\right),\ g_5(0) = -Bi(1 - g_4),\ Nbg_5 + Ntg_7 = 0,\ g_8(0) = 1, \\ &g_1(\infty) \to 0,\ g_4(\infty) \to 0,\ g_6(\infty) \to 0,\ g_8(\infty) \to 0. \end{aligned} \tag{28}$$

3.1.1. Validation of results

Form the current results and published literature observed a good agrement between the results as shown in Table 1.

Table 1. Comparision of skin friction for various magnitudes of in limiting cases when $\lambda = 0, \mathrm{Nr} = \mathrm{Nc} = 0, \mathrm{Rd} = 0, \mathrm{Q}_E = Q_T = E = Pe = Lb = 0, M = 0$.

γ	Current result	Sahoo and Do [59]	Wang [60]	Noghrehabadi *et al.* [61]
0.0	1.00000000	1.001154	1.0	1.000000
1.0	0.430163	0.428450	0.430	0.430160
2.0	0.283982	0.282893	0.284	0.283982
5.0	0.144851	0.144430	0.145	0.144843
20	0.043797	0.0433748	0.0438	0.043794

3.2. Results and discussion

Here, the impact of distinct parameters upon the distribution of velocity $f'(\xi)$, temperature distribution $\theta(\xi)$, concentration $\phi(\xi)$, and motile microorganisms $\chi(\xi)$ are discussed. the parameters are taken in rang $0.1 \le \lambda \le 1.2$, $1.0 \le \alpha \le 4.0$, $0.1 \le M \le 1.2$, $0.1 \le Nc \le 1.2$, $0.1 \le Nr \le 1.2$, $2.0 \le Pr \le 5.0$, $1.5 \le \theta_w \le 1.8$, $0.1 \le Q_E \le 1.2$, $0.1 \le Q_T \le 3.0$, $1.2 \le Le \le 2.4$, $0.1 \le Nt \le 0.4$, $0.1 \le Nb \le 0.4$, $0.1 \le Pe \le 1.2$, $1.2 \le Lb \le 2.4$ and $5.0 \le Br \le 20.0$.

3.2.1. Consequence of velcoity field

The impact of the mixed convection parameter λ upon the flow component f' is shown in Figure 2. The dimensionless velocity f' enhance as mixed convective number λ rises. The behavior of unsteadiness parameter α upon the velocity component f' is illustrated in Figure 3. The dimensionless velocity f' of fluid decays with the growing unsteadiness parameter. Impact of magnetic parameter M versus velocity field is demonstrated in Figure 4. The dimensionless velocity f' of fluid decays with enhancing M. Physically by increassiing the magnetic parameter Lorentz forces are produces causes the resistaance in flow of fluid. Therefore velocity flow is declines. Due to magnetic effect momentum layer vanish. Impact of Bioconvection Rayleigh number Nc on dimensionless velocity gradient f' is captured in Figure 5. Bioconvection Rayleigh number includes density difference that produce a decay in the velocity field. With increase in Nc decreases the velocity f' of fluid. Physically buoyancy forces are develop in the occurrence of higher buoyancy ratio parameter as a result bioconvection, an enhancement bioconvection Rayleigh number reduce the fluid flow. Figure 6 depicts the effect of buoyancy ratio parameter Nr upon velocity field f'. For greater worth of Nr the velocity of the fluid decreases. Parameter of Buoyancy ratio Nr involves density differences. These density differences are responsible for decrease in velocity.

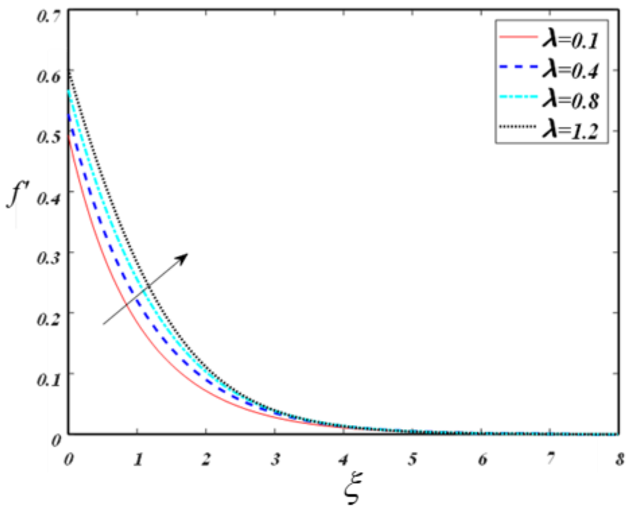

Figure 2. $f'(\xi)$ via λ.

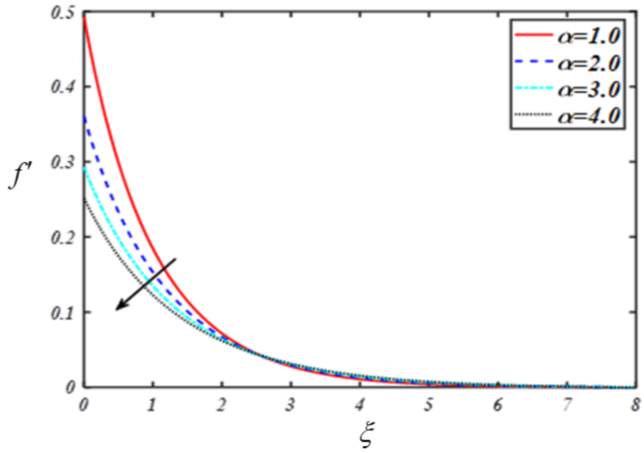

Figure 3. $f'(\xi)$ via α.

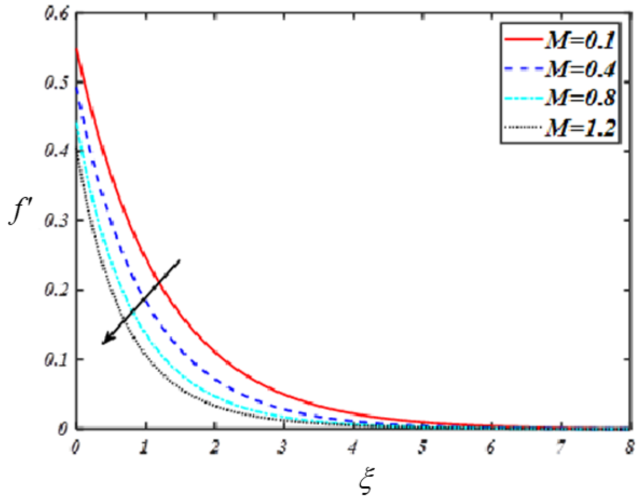

Figure 4. $f'(\xi)$ via M.

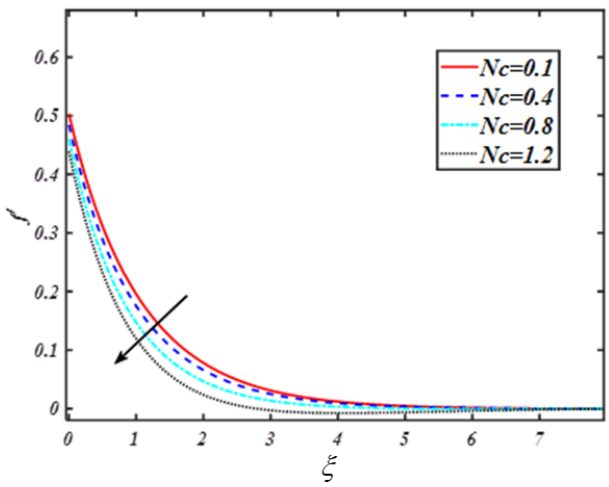

Figure 5. $f'(\xi)$ due to Nc.

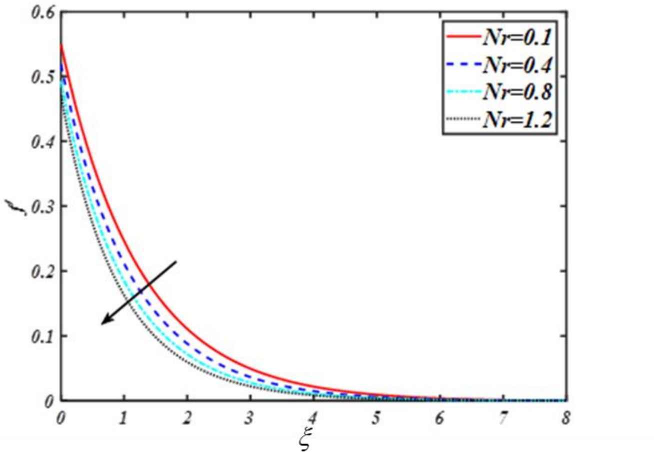

Figure 6. $f'(\xi)$ via Nr.

3.3. Concoquence of temperature distribution

Figure 7 showed the outcome of Prandtl number $\Pr$ against temperature field $\theta(\xi)$. There is an inverse relationship between Prandtl number $\Pr$ on thermal field $\theta(\xi)$. Larger value of $\Pr$ shows lower thermal diffusivity due to which a decay in temperature distribution θ is noted. Temperature distribution $\theta(\xi)$ and dimensionless temperature ratio θ_w has direct relation which is shown in Figure 8. By boosting the value of θ_w the temperature profile θ also increase. More details can be seen in Figures 9 and 10.

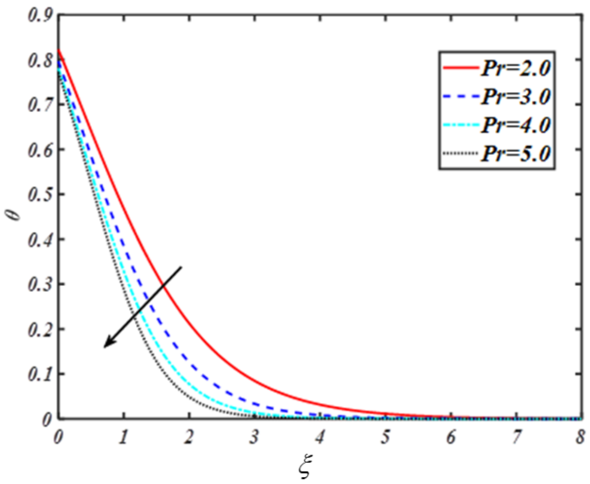

Figure 7. $\theta(\xi)$ via $\Pr$.

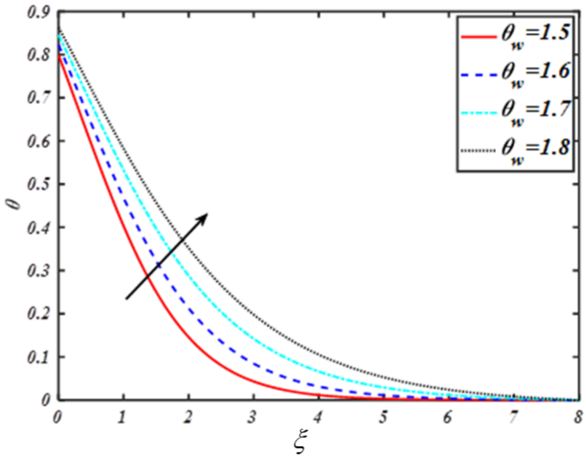

Figure 8. $\theta(\xi)$ via θ_w.

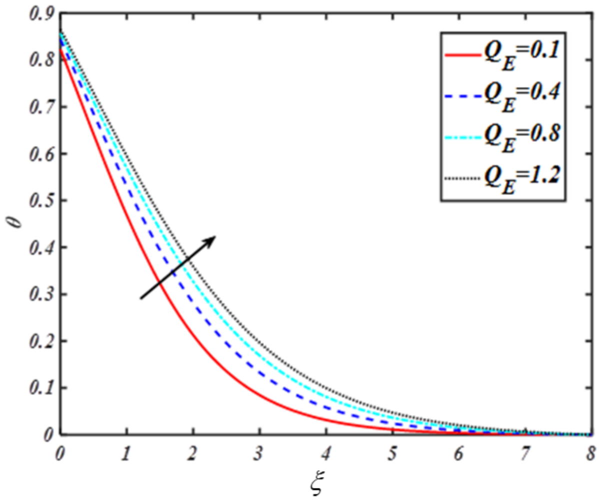

Figure 9. $\theta(\xi)$ via Q_E.

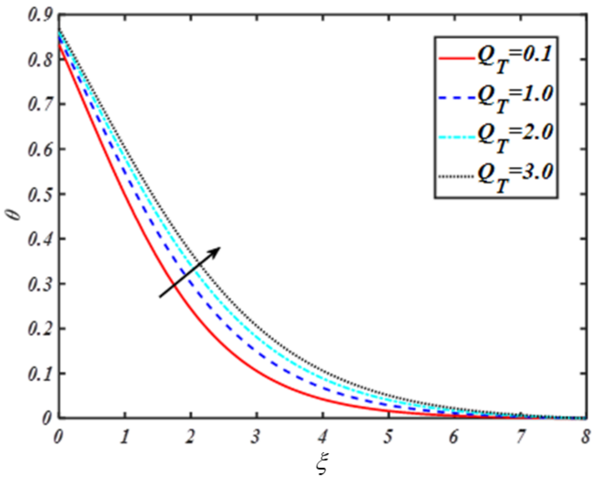

Figure 10. $\theta(\xi)$ via Q_T.

3.4. Concequence of volumetric concentration of nanoparticles

Notable effect of Pr on concentration $\phi(\xi)$ is captured via Figrue 11. It is assumed that an increase in Pr causes reduction in nanoparticle's volumetric concentration. The high value of Prandtl number Pr generates low thermal diffusivity which causes the reduction in solutal field. The physical feature of Lewis number Le and solutal field $\phi(\xi)$ are described in Figrue 12. As the value of dimensionless Lewis number Le increases, the solutal field gradually start decreasing. Figrue 13 indicate the effect of activation energy E on solutal field $\phi(\xi)$. It is concluded that the larger value of activation energy E corresponds to smaller rate of reaction. That's why the chemical process becomes slow down and concentration of nanoparticles increases. Figrue 14 demonstrates the behaviour of thermophoresis variable Nt and concentration field $\phi(\xi)$. The concentration profile $\phi(\xi)$ enhanced with the higher amount of thermophoresis variable Nt. Physically, the thermophoresis phenomenon occurs as a result of nanoparticles moving from hot region to cold region which causes the resulting nanoparticle's percentage to rise. The impact of Brownian motion variable Nb over solutl field $\phi(\xi)$ is illustrated in Figrue 15. The inverse relationship is observed between Nb and $\phi(\xi)$. Actually, the Brownian effect push the nanoparticles in opposite direction of concentration gradient. Larger the Brownian motion variable, lower the solutal field of nanofluid.

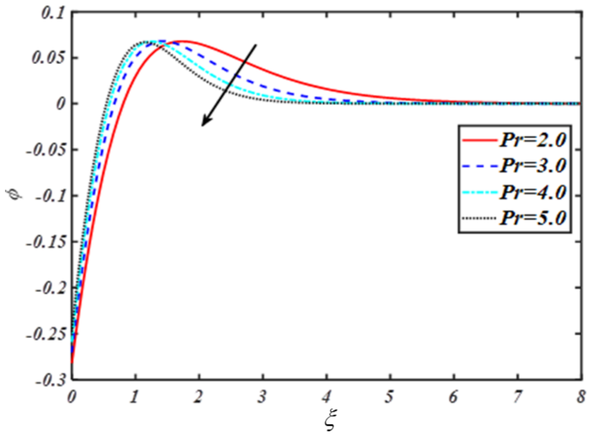

Figure 11. Pr on $\phi(\xi)$.

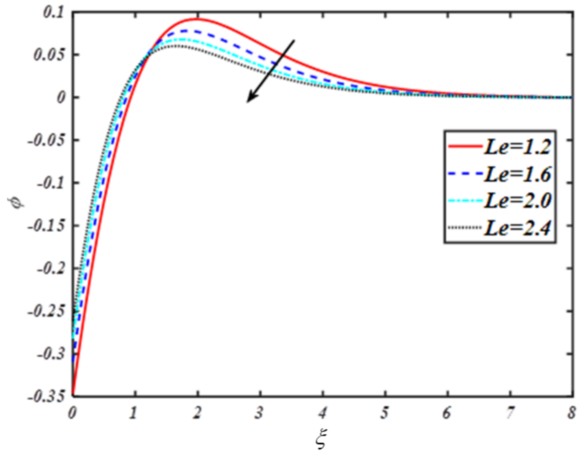

Figure 12. Le on $\phi(\xi)$.

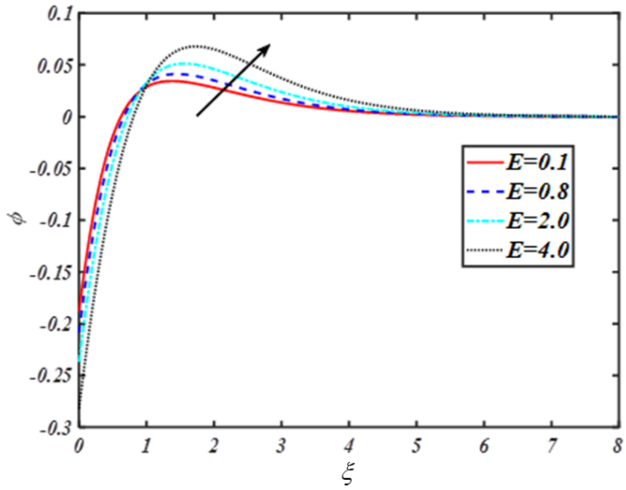

Figure 13. E on $\phi(\xi)$.

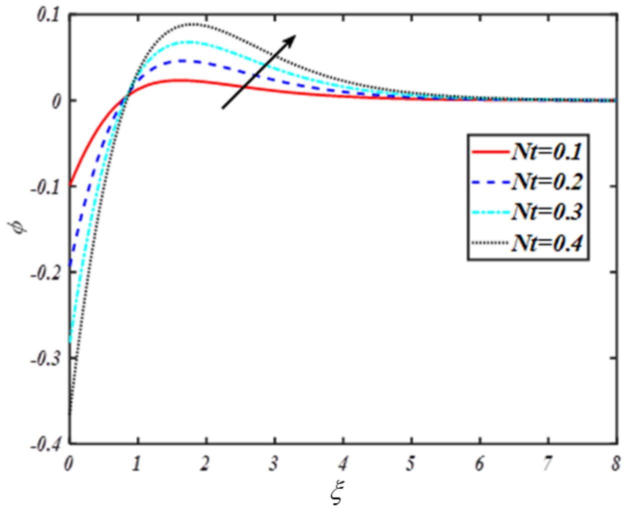

Figure 14. $\phi(\xi)$ via Nt.

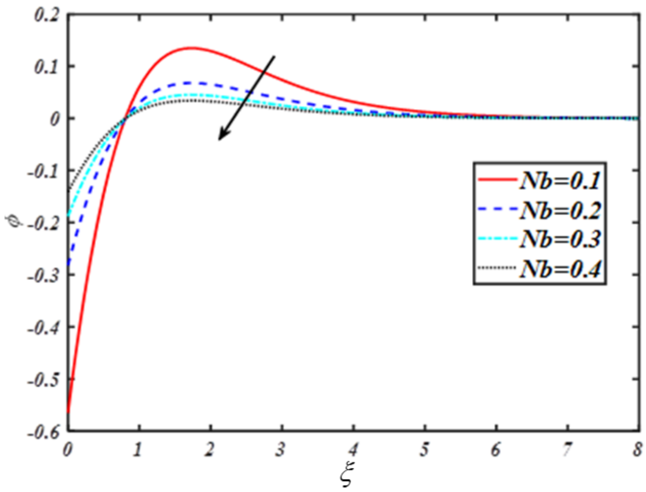

Figure 15. Nb on $\phi(\xi)$.

3.5. Consequence of microorganisms profile

Figure 16 present the consequence of Peclet number Pe over the motile microorganisms concentration profile $\chi(\xi)$. A reduction in microorganisms profile is noticed by changing the value of Pe. Due to bioconvection effect in Pe, the motile microorganisms concentration decreases. The calculation of relative direction strength and hypazard swimming of microorganisms is what the Peclet number actually means. Therefore, a higher Peclet number indicates a more directional movement of the microbe, which results in a smaller motile microorganism field. The consequence of bioconvection Lewis number Lb on the motile microorganisms field $\chi(\xi)$ is demonstrated via Figure 17. The higher bioconvection Lewis number Lb results in decreasing microorganisms profile $\chi(\xi)$.

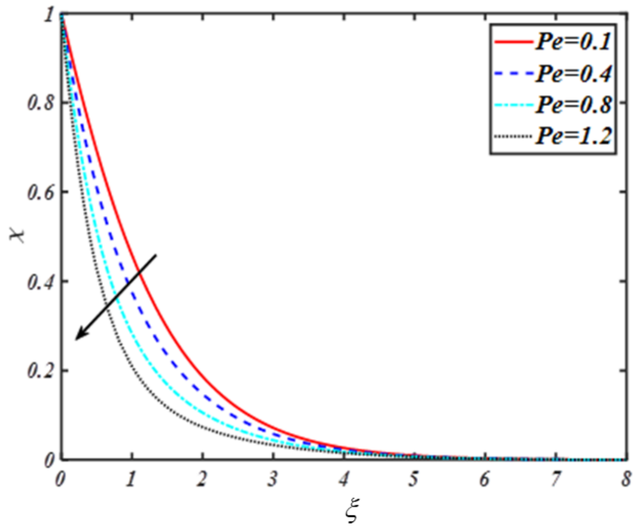

Figure 16. $\chi(\xi)$ via Pe.

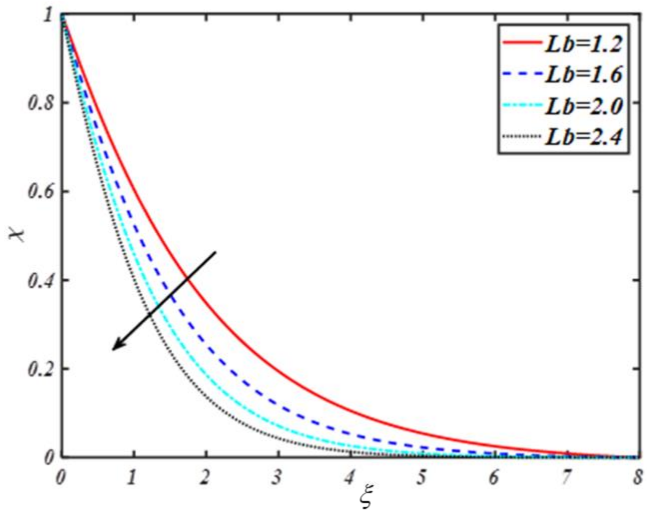

Figure 17. $\chi(\xi)$ via Lb.

3.6. Consequence of entropy generation

Figure18 demonstrates the behaviour of entropy generation N_g via mixed convection parameter γ. There is direct relationship between mixed convection and entropy generation. The increasing value of mixed convection parameter γ boosts up entropy generation N_g. The behaviour of entropy generation N_g via unsteadiness parameter α is illustrated in Figure 19. It shows the inverse relation of α with N_g. The higher value of unsteadiness parameter reduce the generation of entropy. Entropy generation N_g via Brinkman number Br is displayed in Figure 20.

It is worth noting that N_g is proportional to Br. Br measured viscous heating affected by conductive heat transfer. Heat transport via molecular conduction outperforms heat yield via viscous impacts. As a result, the entropy of the system rises.

The skin friction coefficient is examined in Figure 21. It is analyzed that the skin friction coefficient improves with growing amounts of mixed convective number. The effects of the Sherwood Number on activation energy *E* and thermophoresis parameter *Nt* are shown in Figure 22. The effects of the *Nu* Nusselt Number $-\theta'(0)$ on thermophoresis parameter *Nt* and Rd are drawn in Figure 23. It is displayed that the Nusselt number diminishes with an increasing in *Nt*.

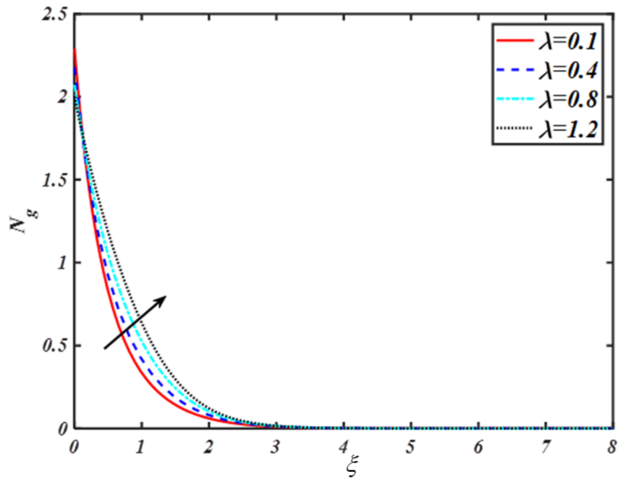

Figure 18. N_g via λ.

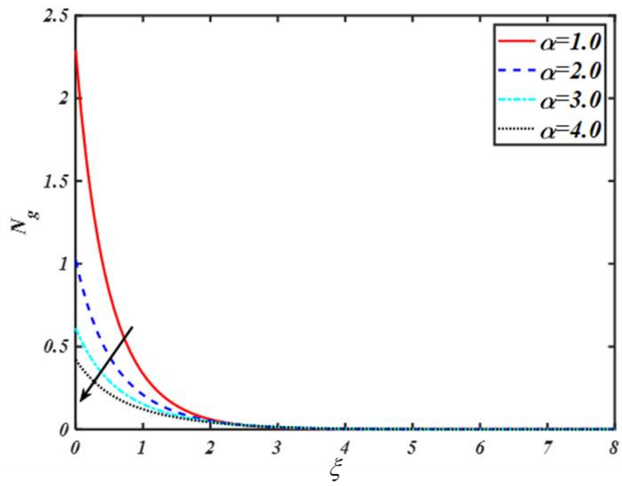

Figure 19. Nature of N_g via α.

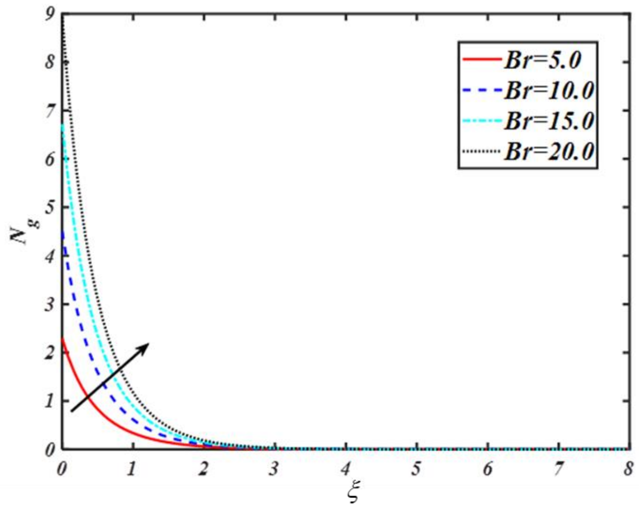

Figure 20. Nature of N_g via Br.

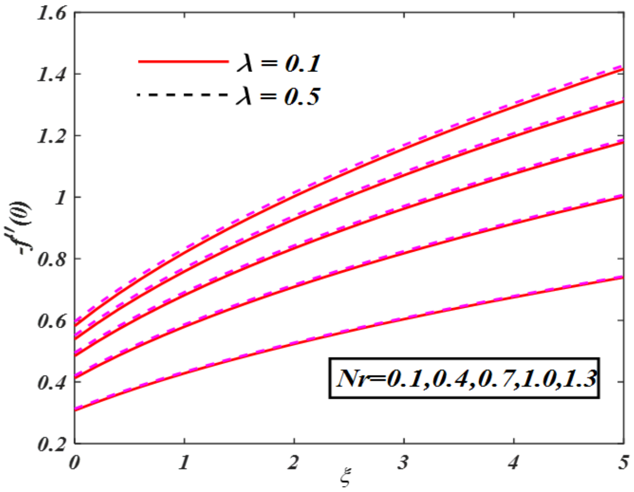

Figure 21. Behaviour of Skin frivtion via N_r and λ.

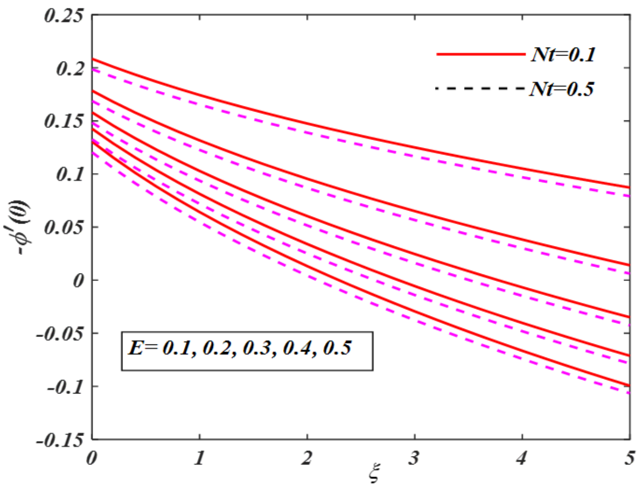

Figure 22. Behaviour of Sherwood Number via Thermophoresis *Nt* and E.

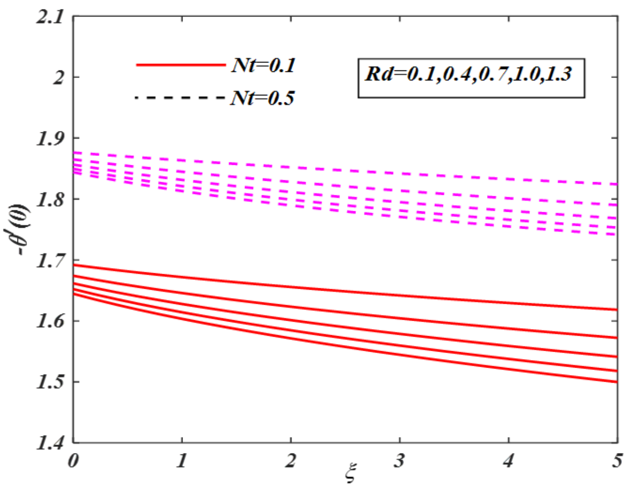

Figure 23. Behaviour of Nusselt Number via *Nt* and *Rd*.

4. Conclusions

The aim of this research is to analyze the impact of exponential based heat source in nanofluid over sheet with gyrotactic motile microorganisms. The effect of nonlinear thermal radiation with entropy of system is also investigated. The major remarks of current article are listed below:

- Greater magnetic parameter causes a reduction in flow of fluid.
- Velocity profile is boosted via larger mixed convection parameter.
- The Prandtl number Pr decreases the thermal distribution.
- The improvements in the radiation parameter, space dependent parameter, and temperature dependent parameter are responsible for the steep enhance in the temperature curve.
- Under the behavior of γ and $Le,$ the concentration function $\varphi(\eta)$ tends to decrease.
- The larger parameter Nt, rise in $\varphi(\eta)$ but it decline with rise in N_b and *S*.
- The microorganisms field is reduced via larger Pe and Lb.

Acknowledgments

This research is supported by Government College University, Faisalabad, Pakistan and Higher Education Commission Pakistan. The authors R. Jarra, H. Shanak, and J. Asad would like to thank Palestine Technical University-Kadoorie for supporting this work financially.

Conflict of interest

No conflict of interests.

References

[1] E. Tombácz, D. Bica, A. Hajdú, E. Illés, A. Majzik, L. Vékás, Surfactant double layer stabilized magnetic nanofluids for biomedical application, *J. Phys.: Condens. Matter*, **20** (2008), 204103. https://doi.org/10.1088/0953-8984/20/20/204103

[2] T. Sharmaa, A. Mohana Reddy, T. Chandra, S. Ramaprabhu, Development of carbon nanotubes and nanofluids based microbial fuel cell, *Int. J. Hydrogen Energ.*, **33** (2008), 749–6754. https://doi.org/10.1016/j.ijhydene.2008.05.112

[3] M. Shaijumon, S. Ramaprabhu, N. Rajalakshmi, Platinum/multi walled carbon nanotubes-platinum/carbon composites as electro catalysts for oxygen reduction reaction in proton exchange membrane fuel cell, *Appl. Phys. Lett.*, **88** (2006), 253105. https://doi.org/10.1063/1.2214139

[4] S. Choi, J. Eastman, Enhancing thermal conductivity of fluids with nanoparticles, *Proceedings of International mechanical engineering congress and exhibition*, 1995, 1–7.

[5] D. Wen, Y. Ding, Formulation of nanofluids for natural convective heat transfer applications, *Int. J. Heat Fluid Fl.*, **26** (2005), 855–864. https://doi.org/10.1016/j.ijheatfluidflow.2005.10.005

[6] J. Buongiorno, Convective transport in nanofluids, *J. Heat Transfer*, **128** (2006), 240–250. https://doi.org/10.1115/1.2150834

[7] S. Murshed, K. Leong, C. Yang, Investigations of thermal conductivity and viscosity of nanofluids, *Int. J. Therm. Sci.*, **47** (2008), 560–568. https://doi.org/10.1016/j.ijthermalsci.2007.05.004

[8] S. Ganguly, S. Sikdar, S. Basu, Experimental investigation of the effective electrical conductivity of aluminum oxide nanofluids, *Powder Technol.*, **196** (2009), 326–330. https://doi.org/10.1016/j.powtec.2009.08.010

[9] A. Kuznetsov, D. Nield, Natural convective boundary-layer flow of a nanofluid past a vertical plate, *Int. J. Therm. Sci.*, **49** (2010), 243–247. https://doi.org/10.1016/j.ijthermalsci.2009.07.015

[10] M. Mustafa, T. Hayat, I. Pop, S. Asghar, S. Obaidat, Stagnation-point flow of a nanofluid towards a stretching sheet, *Int. J. Heat Mass Tran.*, **54** (2011), 5588–5594. https://doi.org/10.1016/j.ijheatmasstransfer.2011.07.021

[11] F. Asadzadeh, M. Nasr Esfahany, N. Etesami, Natural convective heat transfer of Fe_3O_4/ethylene glycol nanofluid in electric field, *Int. J. Therm. Sci.*, **62** (2012), 114–119. https://doi.org/10.1016/j.ijthermalsci.2011.11.010

[12] T. Hayat, M. Waqas, S. Shehzad, A. Alsaedi, A model of solar radiation and Joule heating in magnetohydrodynamic (MHD) convective flow of thixotropic nanofluid, *J. Mol. Liq.*, **215** (2016), 704–710. https://doi.org/10.1016/j.molliq.2016.01.005

[13] M. Farooq, M. Ijaz Khan, M. Waqas, T. Hayatb, A. Alsaedi, M. Imran Khan, MHD stagnation point flow of viscoelastic nanofluid with non-linear radiation effects, *J. Mol. Liq.*, **221** (2016), 1097–1103. https://doi.org/10.1016/j.molliq.2016.06.077

[14] M. Bhatti, A. Zeeshan, R. Ellahi, Simultaneous effects of coagulation and variable magnetic field on peristaltically induced motion of Jeffrey nanofluid containing gyrotactic microorganism, *Microvasc Res.*, **110** (2017), 32–42. https://doi.org/10.1016/j.mvr.2016.11.007

[15] M. Ijaz Khan, T. Hayat, M. Imran Khan, A. Alsaedi, Activation energy impact in nonlinear radiative stagnation point flow of Cross nanofluid, *Int. Commun. Heat Mass*, **91** (2018), 216–224. https://doi.org/10.1016/j.icheatmasstransfer.2017.11.001

[16] S. Nadeem, N. Abbas, A. Khan, Characteristics of three dimensional stagnation point flow of Hybrid nanofluid past a circular cylinder, *Results Phys.*, **8** (2018), 829–835. https://doi.org/10.1016/j.rinp.2018.01.024

[17] M. Bhatti, H. Öztop, R. Ellahi, I. Sarris, M. Doranehgard, Insight into the investigation of diamond (C) and Silica (SiO_2) nanoparticles suspended in water-based hybrid nanofluid with application in solar collector, *J. Mol. Liq.*, **357** (2022), 119134. https://doi.org/10.1016/j.molliq.2022.119134

[18] M. Bhatti, O. Bég, S. Abdelsalam, Computational framework of magnetized MgO-Ni/water-based stagnation nanoflow past an elastic stretching surface: application in solar energy coatings, *Nanomaterials*, **12** (2022), 1049. https://doi.org/10.3390/nano12071049

[19] M. Rashidi, M. Alhuyi Nazari, I. Mahariq, N. Ali, Modeling and sensitivity analysis of thermal conductivity of ethylene glycol-water based nanofluids with Alumina nanoparticles, *Exp. Tech.*, in press. https://doi.org/10.1007/s40799-022-00567-4

[20] S. Rawat, H. Upreti, M. Kumar, Numerical study of activation energy and thermal radiation effects on Oldroyd-B nanofluid flow using the Cattaneo-Christov double diffusion model over a convectively heated stretching sheet, *Heat Transf.*, **50** (2021), 5304–5331. https://doi.org/10.1002/htj.22125

[21] A. Mishra, H. Upreti, A comparative study of Ag-MgO/water and Fe_3O_4-$CoFe_2O_4$/EG-water hybrid nanofluid flow over a curved surface with chemical reaction using Buongiorno model, *Partial Differential Equations in Applied Mathematics*, **5** (2022), 100322. https://doi.org/10.1016/j.padiff.2022.100322

[22] H. Upreti, A. Pandey, S. Rawat, M. Kumar, Modified Arrhenius and thermal radiation effects on three-dimensional magnetohydrodynamic flow of carbon nanotubes nanofluids over bi-directional stretchable surface, *Journal of Nanofluids*, **10** (2021), 538–551. https://doi.org/10.1166/jon.2021.1804

[23] H. Upreti, M. Kumar, Influence of non-linear radiation, Joule heating and viscous dissipation on the boundary layer flow of MHD nanofluid flow over a thin moving needle, *Multidiscip. Model. Ma.*, **16** (2020), 208–224. https://doi.org/10.1108/MMMS-05-2019-0097

[24] A. Pandey, H. Upreti, Mixed convective flow of Ag-H_2O magnetic nanofluid over a curved surface with volumetric heat generation and temperature-dependent viscosity, *Heat Transf.*, **50** (2021), 7251–7270. https://doi.org/10.1002/htj.22227

[25] H. Upreti, N. Joshi, A. Pandey, S. Rawat, Assessment of convective heat transfer in Sisko fluid flow via stretching surface due to viscous dissipation and suction, *Nanosci. Technol.*, **13** (2022), 31–44. https://doi.org/10.1615/NanoSciTechnolIntJ.2022039531

[26] N. Joshi, H. Upreti, A. Pandey, MHD Darcy-Forchheimer Cu-Ag/H_2O-$C_2H_6O_2$ hybrid nanofluid flow via a porous stretching sheet with suction/blowing and viscous dissipation, *Int. J. Comput. Meth. En.*, **23** (2022), 527–535. https://doi.org/10.1080/15502287.2022.2030426

[27] H. Upreti, S. Rawat, M. Kumar, Radiation and non-uniform heat sink/source effects on 2D MHD flow of CNTs-H_2O nanofluid over a flat porous plate, *Multidiscip. Model. Ma.*, **16** (2020), 791–809. https://doi.org/10.1108/MMMS-08-2019-0153

[28] N. Joshi, A. Pandey, H. Upreti, M. Kumar, Mixed convection flow of magnetic hybrid nanofluid over a bidirectional porous surface with internal heat generation and a higher-order chemical reaction, *Heat Transf.*, **50** (2021), 3661–3682. https://doi.org/10.1002/htj.22046

[29] S. Rawat, H. Upreti, M. Kumar, Thermally stratified nanofluid flow over porous surface cone with Cattaneo-Christov heat flux approach and heat generation (or) absorption, *SN Appl. Sci.*, **2** (2020), 302. https://doi.org/10.1007/s42452-020-2099-3

[30] S. Rawat, S. Negi, H. Upreti, M. Kumar, A non-Fourier's and non-Fick's approach to study MHD mixed convective copper water nanofluid flow over flat plate subjected to convective heating and zero wall mass flux condition, *Int. J. Appl. Comput. Math.*, **7** (2021), 246. https://doi.org/10.1007/s40819-021-01190-4

[31] A. Bejan, A study of entropy generation in fundamental convective heat transfer, *J. Heat Transfer*, **101** (1979), 718–725. https://doi.org/10.1115/1.3451063

[32] A. Bejan, Second law analysis in heat transfer, *Energy*, **5** (1980), 720–732. https://doi.org/10.1016/0360-5442(80)90091-2

[33] A. Bejan, Method of entropy generation minimization, or modeling and optimization based on combined heat transfer and thermodynamics, *Revue Générale de Thermique*, **35** (1996), 637–646. https://doi.org/10.1016/S0035-3159(96)80059-6

[34] S. Tasnim, M. Shohel, M. Mamun, Entropy generation in a porous channel with hydromagnetic effect, *Exergy*, **2** (2002), 300–308. https://doi.org/10.1016/S1164-0235(02)00065-1

[35] S. Mahmud, R. Fraser, The second law analysis in fundamental convective heat transfer problems, *Int. J. Therm. Sci.*, **42** (2003), 177–186. https://doi.org/10.1016/S1290-0729(02)00017-0

[36] R. Ellahi, M. Hassan, A. Zeeshan, Shape effects of nanosize particles in nanofluid on entropy generation, *Int. J. Heat Mass*, **81** (2015), 449–456. https://doi.org/10.1016/j.ijheatmasstransfer.2014.10.041

[37] G. Shit, R. Haldar, S. Mandal, Entropy generation on MHD flow and convective heat transfer in a porous medium of exponentially stretching surface saturated by nanofluids, *Adv. Powder Technol.*, **28** (2017), 1519–1530. https://doi.org/10.1016/j.apt.2017.03.023

[38] M. Sheikholeslami, M. Jafaryar, A. Shafee, Z. Li, R. Ul Haq, Heat transfer of nanoparticles employing innovative turbulator considering entropy generation, *Int. J. Heat Mass*, **136** (2019), 1233–1240. https://doi.org/10.1016/j.ijheatmasstransfer.2019.03.091

[39] P. Biswal, T. Basak, Entropy generation vs energy efficiency for natural convection based energy flow in enclosures and various applications: a review, *Renew. Sust. Energ. Rev.*, **80** (2017), 1412–1457. https://doi.org/10.1016/j.rser.2017.04.070

[40] T. Hayat, S. Nawaz, A. Alsaedi, Entropy generation in peristalsis with different shapes of nanomaterial, *J. Mol. Liq.*, **248** (2017), 447–458. https://doi.org/10.1016/j.molliq.2017.10.058

[41] T. Hayat, S. Farooq, B. Ahmad, A. Alsaedi, Effectiveness of entropy generation and energy transfer on peristaltic flow of Jeffrey material with Darcy resistance, *Int. J. Heat Mass*, **106** (2017), 244–252. https://doi.org/10.1016/j.ijheatmasstransfer.2016.10.017

[42] M. Ijaz Khan, S. Qayyum, T. Hayata, M. Waqas, M. Imran Khan, A. Alsaedi, Entropy generation minimization and binary chemical reaction with Arrhenius activation energy in MHD radiative flow of nanomaterial, *J. Mol. Liq.*, **259** (2018), 274–283. https://doi.org/10.1016/j.molliq.2018.03.049

[43] M. Bhatti, M. Sheikholeslami, A. Shahid, M. Hassan, T. Abbas, Entropy generation on the interaction of nanoparticles over a stretched surface with thermal radiation, *Colloid. Surfaces A*, **570** (2019), 368–376. https://doi.org/10.1016/j.colsurfa.2019.03.058

[44] A. Kumar, R. Tripathi, R. Singh, Entropy generation and regression analysis on stagnation point flow of Casson nanofluid with Arrhenius activation energy, *J. Braz. Soc. Mech. Sci. Eng.*, **41** (2019), 306. https://doi.org/10.1007/s40430-019-1803-y

[45] F. Sultan, W. Khan, M. Ali, M. Shahzad, H. Sun, M. Irfan, Importance of entropy generation and infinite shear rate viscosity for non-Newtonian nanofluid, *J. Braz. Soc. Mech. Sci. Eng.*, **41** (2019), 439. https://doi.org/10.1007/s40430-019-1950-1

[46] A. Ullah, Z. Shah, P. Kumam, M. Ayaz, S. Islam, M. Jameel, Viscoelastic MHD nanofluid thin film flow over an unsteady vertical stretching sheet with entropy generation, *Processes*, **7** (2019), 262. https://doi.org/10.3390/pr7050262

[47] M. Nayak, A. Abdul Hakeem, B. Ganga, M. Ijaz Khan, M. Waqas, O. Makinde, Entropy optimized MHD 3D nanomaterial of non-Newtonian fluid: a combined approach to good absorber of solar energy and intensification of heat transport, *Comput. Meth. Prog. Bio.*, **186** (2020), 105131. https://doi.org/10.1016/j.cmpb.2019.105131

[48] N. Khan, I. Riaz, M. Hashmi, S. Musmar, S. Khan, Z. Abdelmalek, et al., Aspects of chemical entropy generation in flow of Casson nanofluid between radiative stretching disks, *Entropy*, **22** (2022), 495. https://doi.org/10.3390/e22050495

[49] G. Shit, S. Mandal, Entropy analysis on unsteady MHD flow of Casson nanofluid over a stretching vertical plate with thermal radiation effect, *Int. J. Appl. Comput. Math.*, **6** (2020), 2. https://doi.org/10.1007/s40819-019-0754-4

[50] R. Vincent, N. Hill, Bioconvection in a suspension of phototactic algae, *J. Fluid Mech.*, **327** (1996), 343–371. https://doi.org/10.1017/S0022112096008579

[51] A. Kuznetsov, Nanofluid bioconvection: interaction of microorganisms oxytactic upswimming, nanoparticle distribution, and heating/cooling from below, *Theor. Comput. Fluid Dyn.*, **26** (2012), 291–310. https://doi.org/10.1007/s00162-011-0230-1

[52] M. Alqarni, S. Yasmin, H. Waqas, S. Khan, Recent progress in melting heat phenomenon for bioconvection transport of nanofluid through a lubricated surface with swimming microorganisms, *Sci. Rep.*, **12** (2022), 8447. https://doi.org/10.1038/s41598-022-12230-4

[53] R. Alluguvelli, C. Balla, K. Naikoti, O. Makinde, Nanofluid bioconvection in porous enclosure with viscous dissipation, *Indian J. Pure Ap. Phy.*, **60** (2022), 78–89.

[54] V. Puneeth, S. Manjunatha, O. Makinde, B. Gireesha, Bioconvection of a radiating hybrid nanofluid past a thin needle in the presence of heterogeneous-homogeneous chemical reaction, *J. Heat Transfer*, **143** (2021), 042502. https://doi.org/10.1115/1.4049844

[55] R. Alluguvelli, C. Balla, K. Naikoti, Bioconvection in porous square cavity containing oxytactic microorganisms in the presence of viscous dissipation, *Discontinuity, Nonlinearity, and Complexity*, **11** (2022), 301–313. https://doi.org/10.5890/DNC.2022.06.009

[56] O. Makinde, I. Animasaun, Thermophoresis and Brownian motion effects on MHD bioconvection of nanofluid with nonlinear thermal radiation and quartic chemical reaction past an upper horizontal surface of a paraboloid of revolution, *J. Mol. Liq.*, **221** (2016), 733–743. https://doi.org/10.1016/j.molliq.2016.06.047

[57] K. Avinash, N. Sandeep, O. Makinde, I. Animasaun, Aligned magnetic field effect on radiative bioconvection flow past a vertical plate with thermophoresis and Brownian motion, *Defect and Diffusion Forum*, **377** (2017), 127–140. https://doi.org/10.4028/www.scientific.net/DDF.377.127

[58] M. Ijaz Khan, S. Ullah, T. Hayata, M. Waqas, M. Imran Khan, A. Alsaedi, Salient aspects of entropy generation optimization in mixed convection nanomaterial flow, *Int. J. Heat Mass*, **126** (2018), 1337–1346. https://doi.org/10.1016/j.ijheatmasstransfer.2018.05.168

[59] B. Sahoo, Y. Do, Effects of slip on sheet-driven flow and heat transfer of a third-grade fluid past a stretching sheet, *Int. Commun. Heat Mass*, **37** (2010), 1064–1071. https://doi.org/10.1016/j.icheatmasstransfer.2010.06.018

[60] C. Wang, Flow due to a stretching boundary with partial slip-an exact solution of the Navier-Stokes equations, *Chem. Eng. Sci.*, **57** (2002), 3745–3747. https://doi.org/10.1016/S0009-2509(02)00267-1

[61] A. Noghrehabadi, M. Saffarian, R. Pourrajab, M. Ghalambaz, Entropy analysis for nanofluid flow over a stretching sheet in the presence of heat generation/absorption and partial slip, *J. Mech. Sci. Technol.*, **27** (2013), 927–937. https://doi.org/10.1007/s12206-013-0104-0